Perpetual Hyperpolarization of Allyl Acetate from Parahydrogen and Continuous Flow Heterogeneous Hydrogenation with Recycling of Unreacted Propargyl Acetate

Tommy Yunpu Zhao,[a] Michelle P. Lapak,[a] Ranjan Behera,[b] Hanqin Zhao,[c] Maria-Jose Ferrer,[a] Helena E. Hagelin Weaver,[c] Wenyu Huang,[b,d] and Clifford R. Bowers[*,a]*

[a]Department of Chemistry and National High Magnetic Field Laboratory, University of Florida, Gainesville, FL 32611

[b]Department of Chemistry, Iowa State University, Ames, IA 50011

[c]Department of Chemical Engineering, University of Florida, Gainesville, FL 32611

[d]Ames Laboratory, U.S. Department of Energy, Ames, IA 50011

Corresponding Author

*Clifford R. Bowers, E-mail: bowers@chem.ufl.edu

Highlights

- The design and demonstration of a closed loop continuous flow packed bed reactor for parahydrogen enhanced nuclear magnetic resonance is presented.
- The reactor system is demonstrated using two types of supported metal nanoparticle catalysts: Rh/TiO_2(anatase) and $Pt_3Sn@mSiO_2$.
- By recirculating the deuterated solvent and unreacted substrate, the closed loop system affords efficient and cost-effective optimization of reaction conditions (e.g., temperature and flow rate) and NMR pulse sequence variables.
- Stable hyperpolarization was observed over a period of 22 minutes with signal enhancements of up to 626 observed at 9.4 T using 99% para-enriched H_2.

Abstract

A novel closed loop, continuous flow (CF) reactor system for parahydrogen enhanced nuclear magnetic resonance (NMR) of liquids via heterogeneous catalysis is introduced which enables recycling of unreacted liquid substrate reactant. This system consists of an HPLC pump, a liquid substrate reservoir incorporating a gas diffuser, an all-metal packed bed catalytic reactor, and an AF-2400 tube-in-tube gas permeable membrane for removal of normal H_2. Two types of supported metal nanoparticle catalysts were tested: mesoporous silica encapsulated Pt_3Sn intermetallic nanoparticles and a Rh on anatase TiO_2 support. In the CF hydrogenation of propargyl acetate to allyl acetate, the hyperpolarized signals exhibited stability over 20 minutes of recirculation, with signal enhancements of up to 626 using 99% p-H_2 and negligible leaching of the catalyst into the flowing solutions. These results demonstrate the practicality of performing systematic optimization of conditions for continuous flow catalysis and polarization transfer to heteronuclei with important implications for biomedical magnetic resonance imaging.

Graphical Abstract

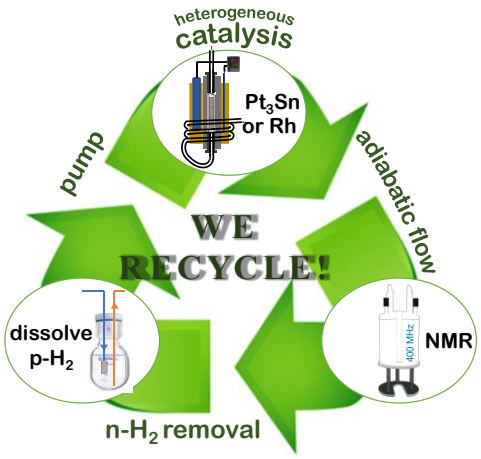

Keywords: parahydrogen, PHIP, heterogeneous catalysis, side-arm hydrogenation, hyperpolarization

1. Introduction

Hyperpolarization from parahydrogen (p-H_2) is gaining traction as a sensitivity enhancement method for in-vivo molecular magnetic resonance imaging [1–5]. A significant breakthrough was the advent of side-arm hydrogenation (SAH), which has extended the reach of the parahydrogen enhanced nuclear magnetic resonance (NMR) technique to molecules not directly producible by hydrogenation, such as acetate and pyruvate [6–11], key biomarkers in the TCA cycle metabolism [7,12]. While promising, SAH and purification have been performed in batch mode where p-H_2 is bubbled through the precursor solution containing the dissolved catalyst. Continuous flow (CF) production of impurity-free hyperpolarized metabolites in solution may be better suited for in-vivo administration for some applications than a single, concentrated, non-physiological bolus [13]. Heterogeneous catalysis is intrinsically compatible with CF production of hyperpolarized liquids, as demonstrated in our recent work [14], which we expand on here.

A few demonstrations of CF hyperpolarization from parahydrogen and homogeneous catalysis have appeared in the literature [15–19]. CF hyperpolarization by heterogeneous catalytic hydrogenation is widely employed for gases [1,20–24]. A hyperpolarized gas stream is produced by flowing the gas mixture containing p-H_2 and an unsaturated substrate through a packed bed reactor containing the solid hydrogenation catalyst. Adapting this configuration to liquid phase reactants would offer greater versatility than batch mode processes. Firstly, the spontaneous separation of liquid substrate and solid catalysts would allow the production of a constant stream of catalyst-free hyperpolarized metabolites. Secondly, the well-controlled contact time, transport time, and reaction temperatures would enable the systematic optimization of conditions for heterogeneous hydrogenation catalysis and non-hydrogenative spin-transfer catalysis processes [25]. Moreover, it would facilitate the robust production of hyperpolarized metabolites with facile in-situ catalyst regeneration. Our group recently demonstrated the feasibility of CF hyperpolarization of liquid SAH precursors by heterogeneous catalysis [14]. Despite the potential advantages, several technical challenges remain to be addressed in the design of the next generation of CF reactor system and high-performance catalysts:

- The reactor materials must withstand the elevated pressures needed to increase the solubility of the gas.
- After hydrogenation, excess dissolved gas should be removed prior to any step-down of the pressure to prevent foaming or bubble formation.
- The packed bed reactor should incorporate a system (e.g., porous frits) to retain the catalyst.

- Reactor systems must withstand the high temperatures (c.a. > 300 °C) necessary for catalyst pre-treatments or regeneration in $O_2/H_2/N_2$ gas streams.
- The reactor should facilitate high catalytic conversion at the requisite flow rates (c.a. > 2.0 mL/min) while maximizing transport and interaction with the catalytic active sites.
- Catalyst materials should be formulated and processed to maximize pairwise addition of parahydrogen to an unsaturated molecule while minimizing leaching into the hyperpolarized liquid stream.
- The volume of the system between the reactor outlet and the NMR probe flow cell, or *dwell volume*, should be as small as possible to minimize the transport time.

Additional requirements necessary for CF SAH include:

- Optimization of the operating conditions to maximize polarization transfer to the heteronucleus of interest (e.g., ^{13}C, ^{15}N) under CF conditions.
- CF chemical cleavage of the side-arm after polarization transfer.

Optimization of the polarization yield and polarization transfer to ^{13}C in such a complex reactor system entails systematic variation of reaction parameters (e.g., flow rate, temperature, precursor concentration) and polarization transfer variables (e.g., magnetic field, transport time, and pulse sequence timings). However, for the targeted flow rate of > 2.0 mL/min, the time-consuming systematic variations would deplete significant volumes of deuterated solvents and isotopically labelled precursors. Considering the high cost of these reagents, recirculation in a closed loop (CL) reactor configuration with a low per-pass catalytic conversion and recycling of unreacted substrate will be both practical and cost-effective. This article presents the details of the design and successful demonstration of such a system using two different types of supported metal nanoparticle hydrogenation catalysts.

2. Materials and Methods

2.1 Closed Loop Packed Bed Flow Reactor Design

Figure 1 displays a block diagram of the versatile closed loop continuous flow (CL-CF) reactor system that achieves continuous hyperpolarization of both liquids and gases at high temperatures and elevated pressures over prolonged periods. The system operates in the ALTADENA mode [26], where hydrogenation adducts formed by p-H_2 addition at low magnetic field in the strong proton-proton spin coupling regime are adiabatically transported to high magnetic field for NMR detection with a 90° RF pulse.

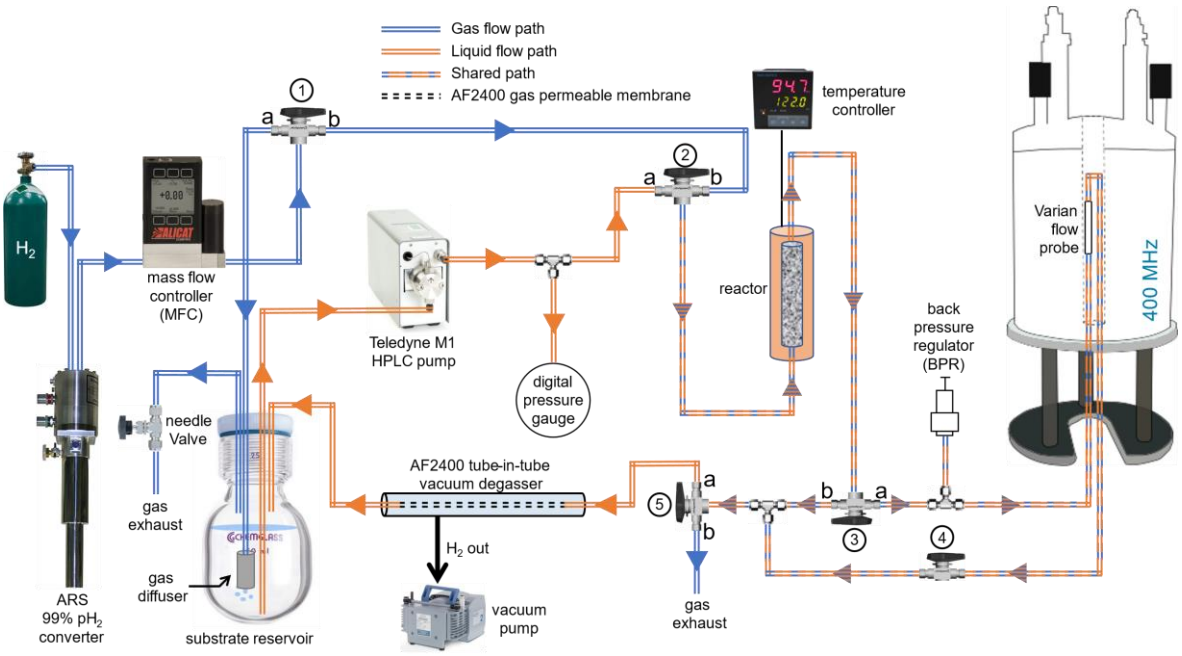

Figure 1. Closed loop continuous flow (CL-CF) ALTADENA reactor system. The blue, orange, and alternating double lines represent the flow path of gas, liquid, or both, respectively. The grey double dashed line represents the AF-2400 gas permeable membrane in the tube-in-tube vacuum degasser. Arrows indicate the flow direction.

Heterogeneous catalysts usually require pre-activation and may require periodic regeneration. Typically, the activation or regeneration cycle involves exposing the catalyst to flowing air for a period of several hours followed by exposure to H_2 diluted in an inert carrier gas (e.g., N_2) at elevated temperature. Supported metal nanoparticles typically require a reduction activation at temperatures of at least 200 °C, whereas temperatures of over 500 °C are needed to induce performance enhancing metal-support interactions [27,28]. Once the catalyst has been activated (or reactivated), exposure to air should be minimized or avoided altogether. Therefore, the system was designed to allow switching between liquid and gas flow paths using three-way valves (labelled 2, 3, and 5 in **Figure 1**), which allows the catalyst to be activated/reactivated in-situ.

A diagram of the all-metal packed bed reactor assembly is shown in **Figure 2**. The ¼-inch outer diameter (O.D.) SS 304 catalyst tube is 80 mm in length. Both ends are terminated with HPLC column end fittings (Valco part #ECEF412.1F) that encapsulate SS 316L porous frits (10 µm pore size, ¼-inch O.D., 1/16-inch thickness, McMaster-Carr part number 9446T31). The Valco fittings on the inlet and outlet of the reactor tube are connected to 30 cm and 10 cm sections, respectively, of 1/16-inch O.D. (0.023-inch I.D.) SS 316 tubing terminating at Swagelok 1/16-inch 3-way valves (2 and 3 in **Figure 1**). The reactor tube is enclosed in a brass heating mantle with a two-piece, clamshell design. The inlet tubing is wound around

the heating mantle body several times to pre-heat the inflowing precursor stream. A heater cartridge (335 W, ½-inch O.D., 1.5-inch length, Omega Engineering, Inc, part number CSH-301335/120V) is inserted into a hole in the heating mantle. The distance between the reactor tube and the heating cartridge is about 1/16-inch. The heating mantle temperature is monitored with a SS jacketed K-type thermocouple inserted into a hole on the opposite side of the reactor tube. The temperature of the brass mantle was controlled with an Omega Engineering CN7223 process controller.

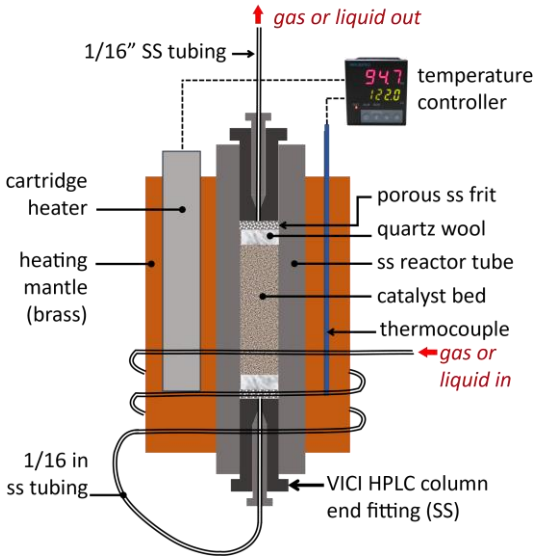

Figure 2. Cross-section of the all-metal packed-bed reactor described in the text.

The 99% para-enriched H_2 was supplied by an Advanced Research Systems (ARS) Model DE-204A cryocooler converter. For the liquid phase CF ALTADENA experiments, the p-H_2 was bubbled at a flow rate of 100 SCCM through 1/16-inch O.D. PEEK (polyether ether ketone) tubing connected to a gas diffuser (solvent filter, 10 µM pore size, IDEX, Mfr # A-550 – Cole Parmer Item # EW-42700-02) that was inserted into the dissolved substrate solution contained in a 48 mL glass pressure vessel (Chemglass Life Sciences, Model 1880-04) at a pressure of 6 bar. A Teledyne M1 HPLC pump was used to drive the circulation of liquid reactant solutions through the packed bed reactor and then into the flow NMR probe. Finally, the liquid flows through the AF-2400 tube-in-tube vacuum degasser to remove unreacted dissolved H_2 and then back to the liquid reservoir. The degasser is the same device used for p-H_2 dissolution in Ref. [14]. Here, the outer tube is evacuated to sub-Torr pressure to extract H_2 from solution.

The efficiency of the AF-2400 vacuum degasser was tested by comparing the concentrations of dissolved H_2 before and after passing an H_2-saturated solution through the device. The test solution containing 100 mM propargyl acetate (PPGA) in d_4-methanol with 0.05 v% of TMS was saturated with

normal H_2 (25 % para) by bubbling at a flow rate of 350 mL/min for 10 min. The degasser was installed at the inlet of the flow probe with a bypass option. The thermally polarized 400 MHz ^{1}H NMR spectra of the PPGA solution acquired with and without bypassing the tube-in-tube device at a flow rate of 2.0 mL/min are shown in Figure 3. The H_2 concentrations were then deduced by comparing the peak integrals of H_2 and the TMS reference. The H_2 concentrations of 3.74 mM and 17.5 mM were obtained with and without degassing, respectively, demonstrating a 78.6% efficiency of H_2 removal.

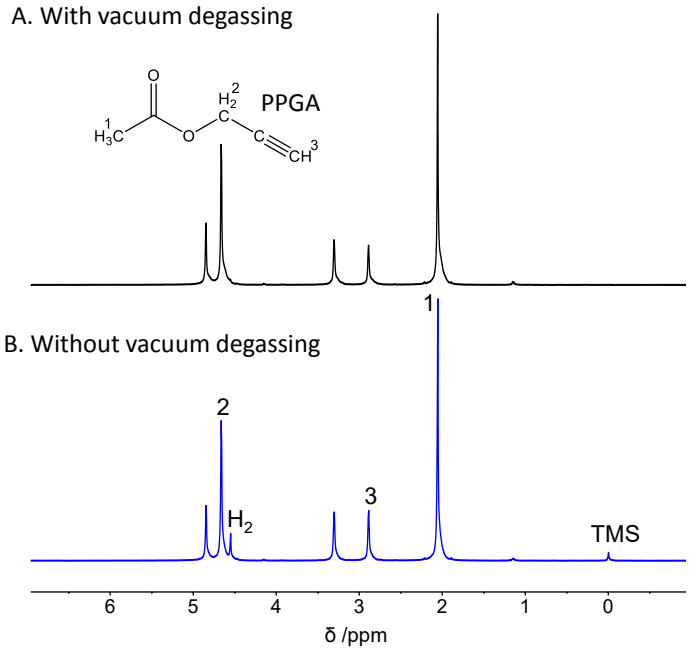

Figure 3. Test results for the AF-2400 tube-in-tube vacuum degasser at a flow rate of 2.0 mL/min. The 400 MHz ^{1}H NMR spectra of a d_4-methanol solution containing 100 mM propargyl acetate (PPGA) saturated with normal H_2 were acquired A) with and B) without the tube-in-tube device inserted into the flow path.

The pressure of the liquid at the inlet of the reactor tube was monitored with a digital pressure gauge. The total dwell volume between the reactor tube outlet to the flow cell is approximately 0.25 mL. The thermally polarized spectrum is acquired under non-flowing conditions by turning valve 3 to position 'b' and closing valve 4. The gas phase hydrogenation and the in-situ catalyst treatment can be conducted by connecting the three-way valves 1, 2 and 5 to position 'b'. Note that the gas cannot recirculate in the CL-CF setup, so the effluent gases are vented to exhaust after a single pass through the catalyst.

For the CL-CF heterogeneous hydrogenation of PPGA, the reactor tube was packed with 22 mg of catalyst, either Pt_3Sn@mSiO_2 or Rh/TiO_2-ANP, synthesized as described below. Solutions containing 100 mM PPGA (Sigma-Aldrich, 98%) in methanol-d_4 (Cambridge Isotope Laboratories, 99.8% D) were prepared by adding 30 mL of substrate solution into the 48 mL liquid reservoir. The solution was sparged with

helium gas at 25 psi for at least 10 min. The 99% p-H_2 was then dissolved by bubbling through the solution at 72 psi for 10 min. Hydrogenation was performed at a magnetic field of 4.5 mT. CL-CF ALTADENA NMR spectra were acquired using a 400 MHz Varian VNMRS spectrometer equipped with a Varian 400 MHz triple resonance H(C/N) IFC flow probe with a coil volume of 60 µL. Several reactor temperatures and liquid flow rates were tested.

2.2 Data Analysis

Per-Pass Conversion

Due to the recirculation of liquid substrate, unreacted substrate molecules will pass through the catalyst bed multiple times prior to hydrogenation. The per-pass conversions to allyl acetate (AA, χ_{AA}^{pp}) and propyl acetate (PPA, χ_{PPA}^{pp}) were calculated using the following equations,

$$\chi_{AA}^{pp} = \frac{\chi_{AA}^{a} - \chi_{AA}^{b}}{n^{pass}} \quad (1)$$

$$\chi_{PPA}^{pp} = \frac{\chi_{PPA}^{a} - \chi_{PPA}^{b}}{n^{pass}} \quad (2)$$

$$n^{pass} = \frac{f \cdot t}{V} \quad (3)$$

The symbol references are defined in **Table 1**.

Table 1. Symbol references in Equations (1-3).

Symbol	Meaning
$\chi_{AA}^{pp}, \chi_{PPA}^{pp}$	Percent conversion to AA and PPA per-pass.
$\chi_{AA}^{a}, \chi_{AA}^{b}$	Percent conversion to AA calculated from the thermally polarized spectrum acquired after and before the current array experiment.
$\chi_{PPA}^{a}, \chi_{PPA}^{b}$	Percent conversion to PPA calculated from the thermally polarized spectrum acquired after and before the current array experiment.
n^{pass}	Number of passes between the acquisition of two thermally polarized spectra.
f	Flow rate of liquid substrate.
t	Circulation time between the acquisition of two thermally polarized spectra.
V	Total volume of liquid substrate in the system.

Enhancement Factor

The observed enhancement factor of H^6 in AA (ε_{AA}) and H^{11} in PPA (ε_{PPA}) were calculated by the following equations:

$$\varepsilon_{AA} = \frac{S_6^{ALT}}{\Delta S_6^{TP}/n^{pass}} \times NS_{TP} \quad (4)$$

$$\varepsilon_{PPA} = -\frac{S_{11}^{ALT}}{\Delta S_{11}^{TP}/3n^{pass}} \times NS_{TP} \quad (5)$$

where S_6^{ALT} and S_{11}^{ALT} represent the peak integral of H^6 and H^{11} in the ALTADENA spectrum, respectively; ΔS_6^{TP} and ΔS_{11}^{TP} represents the peak integral increment of H^6 and H^{11}, respectively, obtained by subtracting the integrals in the thermally polarized spectrum acquired before the array experiment from that after the array experiment. NS_{TP} is 32 and 8 for experiments using $Pt_3Sn@mSiO_2$ and Rh/TiO_2-ANP catalysts, respectively.

Polarization Yield

The polarization yield is the product of the conversion and signal enhancement factor, $\chi^{pp} \cdot \varepsilon$.

2.3 Catalysts

Synthesis of $Pt_3Sn@mSiO_2$ Intermetallic Nanoparticles

The mesoporous silica encapsulated Pt_3Sn intermetallic nanoparticles ($Pt_3Sn@mSiO_2$ iNPs) were synthesized by a method reported in our previous study [29]. 8.4 g of tetradecyltrimethyl-ammonium bromide (TTAB) was dissolved in 200 mL DI water in a 500 mL round-bottomed flask. In a centrifuge tube, 104 mg of potassium tetrachloroplatinate (II) (K_2PtCl_4) was dissolved in 25 mL DI water which was added to the above TTAB solution. A septum was used to cap the round-bottomed flask. The solution was stirred at room temperature at 600 rpm for 10 min and then moved to an oil bath preheated to 50 °C and stirred for another 10 min until the solution became clear. To this, a freshly prepared ice-cold sodium borohydride ($NaBH_4$) solution (284 mg $NaBH_4$ in 25 mL DI water) was added using a syringe. Excess hydrogen generated was vented out of the solution. The solution was allowed to stir at 50 °C for 24 h, which resulted in the formation of a dark brown colloidal solution of Pt nanoparticles (NPs). This solution was centrifuged at 4000 rpm four times for 30 min each, discarding the residue after each session. Finally, the supernatant was centrifuged at 12000 rpm for 15 min twice, collected, and dispersed in 200 mL of aqueous solution and placed in an oil bath at 50 °C. The pH of this solution was adjusted to 10-11 by adding 0.05 M NaOH solution. A solution of 600 µL of tetraethylorthosilicate (TEOS) dissolved in 5.4 mL methanol solution was added dropwise under stirring. After 3 h, the sample was centrifuged at 12000 rpm

twice, and the coated Pt particles (Pt@mSiO$_2$) were redispersed in methanol. The surfactant was removed via refluxing in 6% HCl acidic methanol solution at 90 °C for 24 h.

In the synthesis of the Pt$_3$Sn@mSiO$_2$ catalyst, the platinum content in Pt@mSiO$_2$ seed particles was obtained using ICP-MS. The Pt@mSiO$_2$ solution was centrifuged and redispersed in 80 mL of tetraethylene glycol in a 250 mL two-neck flask. An appropriate amount of $SnCl_2 \cdot 2H_2O$ was then added, ensuring a Pt:Sn molar ratio of 3:1. The solution was sonicated to obtain a homogeneous mixture. After removing air from the flask and refilling with Ar gas, the flask was heated using a temperature-controlled heating mantle to 280 °C and then maintained for 2 h. The obtained alloy was centrifuged, washed, and dried, before annealing/reducing at 600 °C in a 10% H_2/Ar flow (50 mL/min total flow rate) in a tube furnace to obtain Pt$_3$Sn@mSiO$_2$ intermetallic nanoparticles.

The core-shell structure of the Pt$_3$Sn@mSiO$_2$ iNPs and the intermetallic phase was confirmed by the STEM (**Figure 4A**) and PXRD (**Figure 4B**), respectively. The average particle size for the Pt$_3$Sn@mSiO$_2$ intermetallic nanoparticles was determined to be 17 nm.

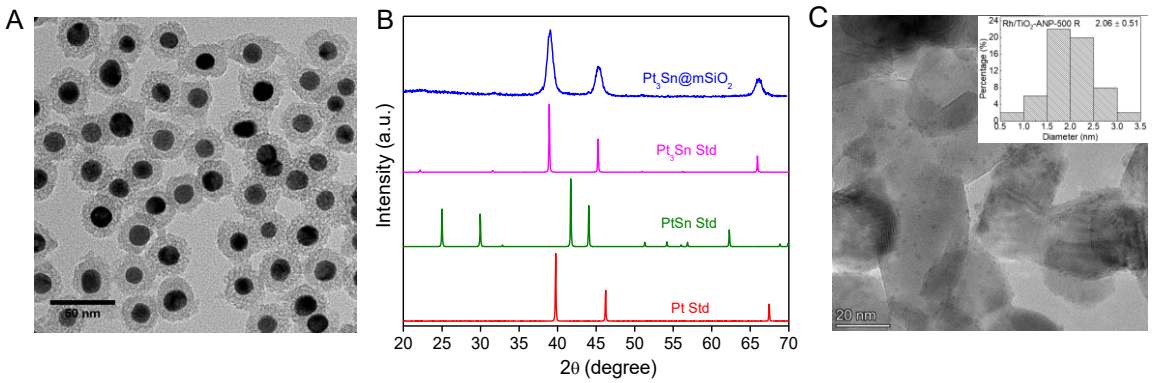

Figure 4. Characterization of Pt$_3$Sn@mSiO$_2$ iNPs. A) Scanning transmission electron microscope (STEM) image. The length-scale bar indicates 50 nm. B) Powder x-ray diffraction (PXRD) peaks of the Pt$_3$Sn@mSiO$_2$ catalyst (in blue) alongside the MDI JADE [30] standard diffraction patterns for Pt (in red, 65-2868), PtSn (in green, 65-0959), and Pt$_3$Sn (in violet 65-0958) confirms the pure phase intermetallic crystal-structure of the catalyst. C. Representative TEM image of the Rh/TiO$_2$-ANP obtained after reduction at 500 °C. The length-scale bar indicates 20 nm. Inset: histogram of measured particle sizes. The average Rh particle size in the TEM image is 2.1 $\pm$ 0.5 nm.

Synthesis of Rh/TiO$_2$-ANP

The Rh/TiO$_2$-ANP catalyst with a target Rh loading of 0.5 wt.% was synthesized by the incipient wetness impregnation (IWI) method. Prior to impregnation, a 1 mL DI water solution consisting of 14 mg $Rh(NO_3)_3 \cdot 6H_2O$ was ultrasonicated for 30 s. Rh precursor solution was incrementally dispensed into the 1 g TiO$_2$-ANP support (anatase titania nanoparticles, Nanostructured & Amorphous Materials, Inc., 99% purity, catalog # 5430-093020), 200 µL at a time. The mixture was dried overnight at 80 °C, followed by

the calcination in air at 350 °C. Temperature programmed reduction (TPR) experiments were then performed from 25 °C to 350 °C at a rate of 10 °C/min. The total heating time was 70 min. A representative TEM image of a similarly prepared Rh/TiO_2-ANP catalyst batch with the same loading is presented in **Figure 4C**. The average diameter of the Rh nanoparticles is estimated to be 2.1 ± 0.5 nm.

3. Results and Discussion

3.1 Flow Rate Studies

CF ALTADENA spectra were acquired every 8 s, 4 s, and 2 s at liquid flow rates of 1.0 mL/min, 2.0 mL/min, and 3.5 mL/min, respectively. For all flow rates, each spectrum was acquired as a single transient with a $\pi/2$ RF pulse and an acquisition time of 0.5 s. The thermally polarized spectrum was acquired immediately following the completion of the arrayed experiment by accumulation of 8 (Rh/TiO_2-ANP) or 32 ($Pt_3Sn@mSiO_2$) transients with a recycle delay of 30 s.

CL-CF heterogeneous hydrogenation of PPGA was performed with 99% p-H_2 using $Pt_3Sn@mSiO_2$ and Rh/TiO_2-ANP catalysts. The catalyst beds were heated to 100 °C and the liquid flow rate was set to 2.0 mL/min. The HPLC pump was activated 4 s prior to the acquisition of the 1st ALTADENA spectrum. **Figures 5A** and **5B** represent the stacked plots of 100 ALTADENA spectra acquired every 4 s during the CF hydrogenation using $Pt_3Sn@mSiO_2$ and Rh/TiO_2-ANP, respectively. In both experiments, the hyperpolarized peaks of AA emerge at the 28th scan (126 s after the start of liquid flow) and stabilize after the 32nd scan, consistent with the approximately 4.0 mL volume between the liquid reservoir to the detection coil. A steady state was attained between the 32nd and the final 100th scan, where the ALTADENA signal exhibits high stability. Hyperpolarized PPA peaks (H^{10} and H^{11}) are observed only in the experiment using the Rh/TiO_2-ANP catalyst, consistent with its lower semi-hydrogenation chemoselectivity.

The conversion and signal enhancement in the CF hydrogenation were obtained by comparing the ALTADENA spectrum to the thermally polarized spectrum acquired under non-flowing conditions immediately after the array experiment. Note that the hydrogenation products are accumulated during the recirculation of substrates. The number of passes (n^{pass}) is estimated from the flow rate (f), circulation time (t), and the total liquid volume (V). The value is used in the calculation of conversion per-pass (χ^{pp}) and the observed enhancement factor (ε).

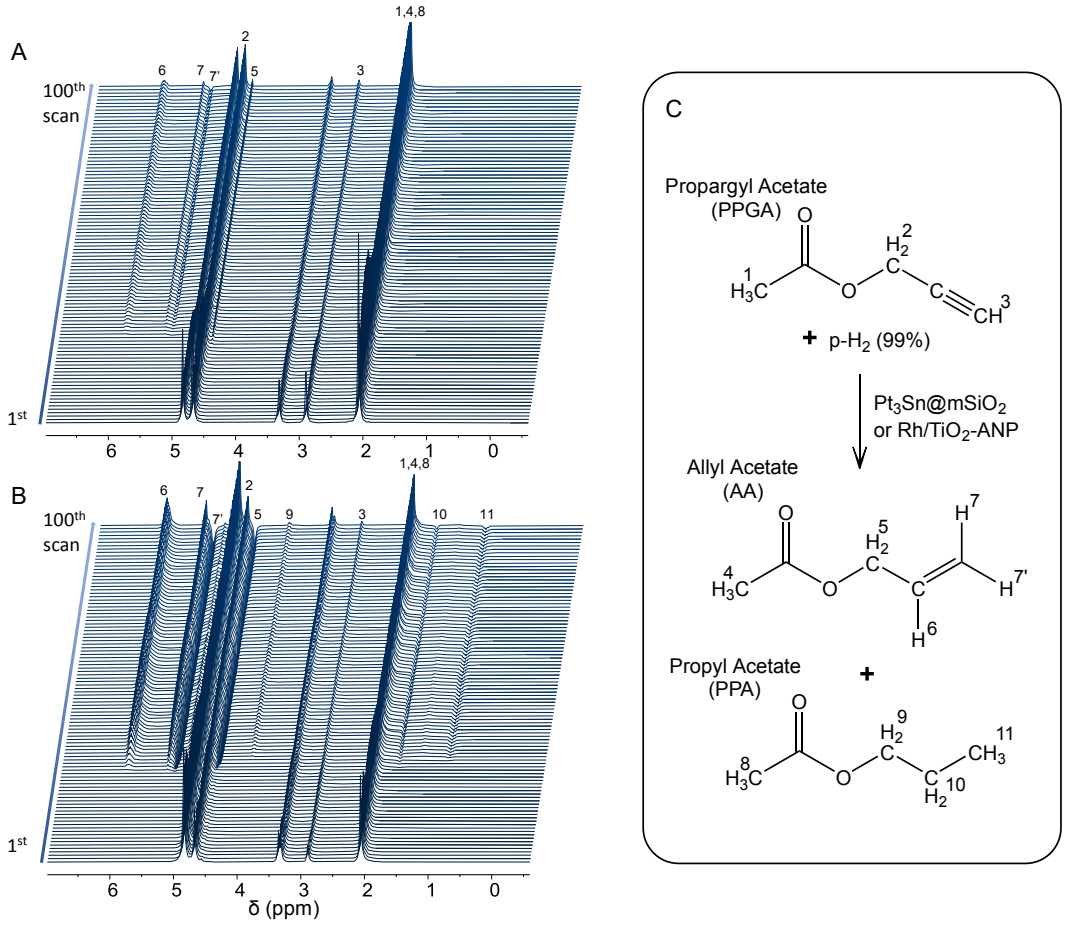

Figure 5. Stacked array of 400 MHz ^{1}H ALTADENA spectra acquired every 4.5 s over the course of CF hydrogenation of PPGA with 99% p-H_2 catalyzed by 22 mg of A) $Pt_3Sn@mSiO_2$ and B) Rh/TiO_2-ANP using CL-CF setup. The reactor temperature was 100 °C and the flow rate was 2.0 mL/min. C) Reaction scheme and proton numbering.

Figures 6A and **6B** show the signal-averaged thermally polarized spectra (upper traces) and the representative CF ALTADENA spectra (lower traces) from experiments using $Pt_3Sn@mSiO_2$ and Rh/TiO_2-ANP, respectively. The results for both catalysts are summarized in **Table 2**. The Rh/TiO_2-ANP exhibits approximately 3 times stronger ALTADENA signal and 10 times stronger thermally polarized signal for H^6 of AA than $Pt_3Sn@mSiO_2$ catalysts, resulting in a lower enhancement factor for the Rh catalyst. The χ^{pp} values of AA using Rh/TiO_2-ANP and $Pt_3Sn@mSiO_2$ are 1.63% and 0.16%, respectively, and the enhancement factors are 80 and 211.8 using 99% p-H_2. The lower conversion and higher signal enhancement obtained using $Pt_3Sn@mSiO_2$ are consistent with the elevated H_2 dissociation barrier and the restricted H diffusion on the Pt_3Sn intermetallic surface that promote the pairwise hydrogenation [31,32]. In addition, the hyperpolarized over-hydrogenated product, PPA, is only observed using the Rh/TiO_2-ANP catalyst, with a conversion of 0.89% and a signal enhancement of 22.5. This demonstrates

the higher chemoselectivity to the alkene product using the $Pt_3Sn@mSiO_2$ catalyst, which is likely due to the low H coverage on the Pt_3Sn surface that inhibits over-hydrogenation [33].

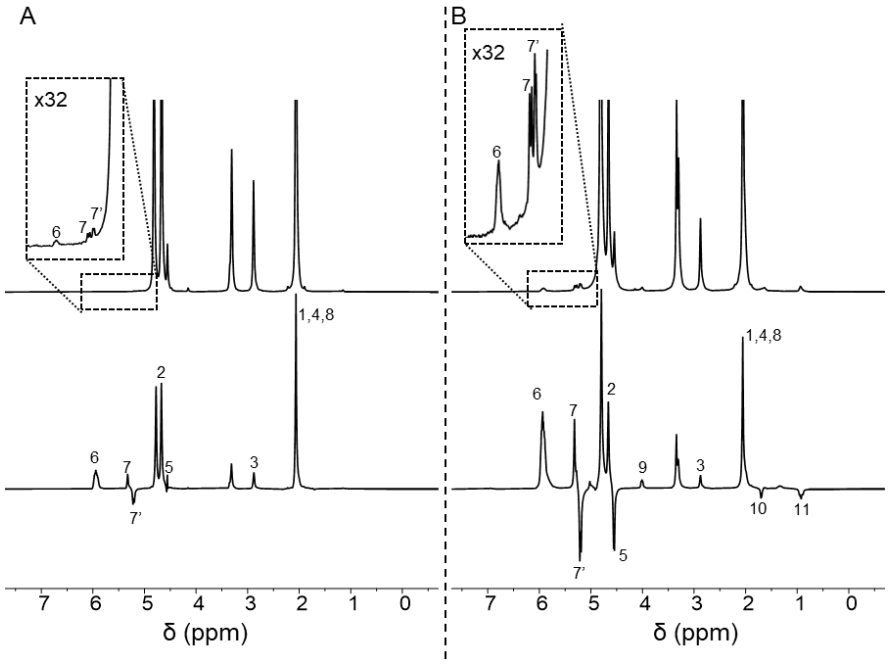

Figure 6. The ^{1}H NMR spectra for the CF hydrogenation of PPGA with 99% p-H_2 catalyzed by A) $Pt_3Sn@mSiO_2$ and B) Rh/TiO_2-ANP using the CL-CF setup. The experiments were conducted at 100 °C with a liquid flow rate of 2.0 mL/min. Lower traces: the representative ALTADENA spectrum from the steady-state region in the array experiment (1 transient). Upper traces: thermally polarized spectrum acquired under the non-flowing condition at the end of the array experiment, 32 transients with a recycle delay of 60 s. All spectra are displayed with the same vertical scale. The peak labels correspond to the proton labeling in **Figure 5.**

Table 2. Per-pass conversion (χ^{pp}), signal enhancement (ε), and polarization yield ($\chi^{pp} \cdot \varepsilon$) in the CF hydrogenation of PPGA to AA and PPA using 99% p-H_2 catalyzed by $Pt_3Sn@mSiO_2$ and Rh/TiO_2-ANP using the CL-CF setup at 100 °C and 2.0 mL/min.

Catalyst	Product	χ^{pp}	ε	$\chi^{pp} \cdot \varepsilon$
$Pt_3Sn@mSiO_2$	AA	0.16% ± 0.001%	212 ± 3	0.34 ± 0.005
Rh/TiO_2-ANP	AA	1.63% ± 0.05%	80.0 ± 0.8	1.43 ± 0.06
	PPA	0.63% ± 0.02%	22.5 ± 0.7	0.16 ± 0.01

The key feature of the CL-CF setup is the highly stable production of a hyperpolarized stream for extended periods of time. The stability of ALTADENA signal during 22.5 min of CF hydrogenation was tested with both $Pt_3Sn@mSiO_2$ and Rh/TiO_2-ANP catalysts. The experiments were conducted at 100 °C and 2.0 mL/min. A total of 300 ALTADENA spectra were collected using a 4.5 s interval. The integrals of H^3 (PPGA, blue circles), H^6 (AA, green diamonds), and H^{11} (PPA, orange squares) are plotted against circulation

time, shown in **Figure 7.** The total volume of substrate was 22 mL, so more than 2 cycles were completed during 22.5 min of flow at 2.0 mL/min.

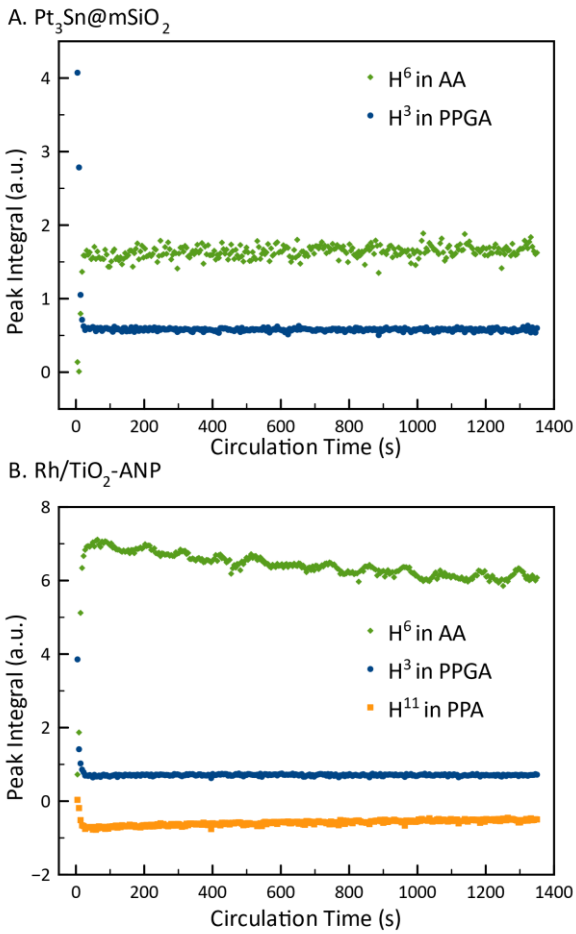

Figure 7. The peak integrals of H^3, H^6, and H^{11} in the CF ALTADENA spectra acquired every 4.5 s over the course of CF hydrogenation reaction at 100 °C and 2.0 mL/min using A) $Pt_3Sn@mSiO_2$ and B) Rh/TiO_2-ANP.

As seen in **Figure 7**, the $Pt_3Sn@mSiO_2$ demonstrates higher stability for both the ALTADENA peak of H^6 and thermally polarized peak of H^3 during the experiment. Due to the lower per-pass conversion, the average integral of the H^3 peak decreases by only 0.8% after 22.5 min circulation, while the average integral of hyperpolarized H^6 peak increased by 4.4%. In addition, the ALTADENA signal exhibits larger fluctuations than the thermally polarized signal. This could be due to fluctuations in temperature and flow rate.

In the experiments with the Rh/TiO_2-ANP catalyst (**Figure 7B**), an obvious decay of the ALTADENA signal integrals is observed for both the H^6 and H^{11} peaks during the CF reaction. The integrals decrease

by 13.3% and 30.4%, respectively, after 22.5 min of circulation, whereas the thermally polarized H^3 peak fluctuates by less than 1%. Therefore, the decrease in the ALTADENA signals cannot be attributed to a change in the surface coverage over the metal nanoparticle surface. The ALTADENA signals stabilize at about 20 min after the start of the flow. The decline is likely due to the approach toward a steady-state para-enrichment in the loop resulting from the incomplete (c.a. 80%, see Supporting Information) removal of para-depleted H_2 by the AF-2400 degasser. The residual para-depleted H_2 would, after mixing, lower the overall enrichment. This effect is of the correct magnitude and timescale to explain the 13% decline in the H^6 ALTADENA signal after approximately two round trips. The greater relative decrease in the H^{11} ALTADENA signal is also consistent with this explanation since the alkane is formed from two equivalents of H_2. In contrast, there is no noticeable decay of the ALTADENA signals in the experiments using $Pt_3Sn@mSiO_2$ catalyst (**Figure 7A**), consistent with the lower activity for para-ortho back conversion for this material.

After the experiment was finished, the reaction mixtures were analyzed by ICP-MS to detect the metal leaching from the heterogeneous catalyst into the recirculated solution. The concentration of Pt and Rh metals in the reaction effluent through $Pt_3Sn@mSiO_2$ and Rh/TiO_2-ANP catalysts was 0 ppb and 16.4 ppb (μg/L), respectively. Apparently, the protective encapsulation of the Pt_3Sn nanoparticles in a mesoporous silica shell makes the metals less prone to leaching than the solvent exposed Rh atoms in the TiO_2-supported nanoparticle catalyst. A contributing factor could be the small size of the Rh nanoparticles, and it is unknown if the leached metal is in the form of detached particles or etched Rh^{3+}. Nevertheless, the total mass of Rh lost to leaching was 0.11 mg, corresponding to only 0.4 % of the total Rh in the 22 mg catalyst sample.

3.2 Variable Reactor Temperature Study

The reaction temperature was varied over several values for the CF hydrogenation of PPGA catalyzed by $Pt_3Sn@mSiO_2$. Experiments were performed with a fixed flow rate of 2.0 mL/min at 100 °C, 80 °C, and 60 °C (in that order) using 22 mg of $Pt_3Sn@mSiO_2$ catalysts and 25 mL of 100 mM PPGA solution in methanol-d_4. At each temperature, an array of 400 ALTADENA spectra were acquired, one every 4.5 s, corresponding to a total circulation time of 30 min and $n^{pass} = 3$. The per-pass conversion was calculated based on the thermally polarized spectra collected before and after completion of the arrayed experiment. Due to the low per-pass conversion for this catalyst, the reactant and product concentration did not change appreciably over the course of the experiment. The signal enhancement was calculated by comparing the ALTADENA signal to the difference in the signal integrals of the corresponding peak in the thermally polarized spectra.

As seen in **Figure 8** and **Table 3**, 100 °C yields the highest ALTADENA signal for the Pt_3Sn@$mSiO_2$ catalyst, with the highest χ_{AA}^{pp} (0.16%) and the ε_{AA} of 211.8. As the temperature decreased to 80 °C, the ALTADENA signal is halved with an 80% decrease of χ_{AA}^{pp} (0.03%), yielding the highest ε_{AA} of 625.9. At 60 °C, the conversion was negligible. The conversion and signal enhancement are inversely correlated with changing temperature, although the effect of temperature on the two parameters is disproportionate. The increase of conversion at higher temperatures can be explained by the increased rate of reaction, while the decrease in signal enhancement can be attributed to the more rapid H_2 diffusion.

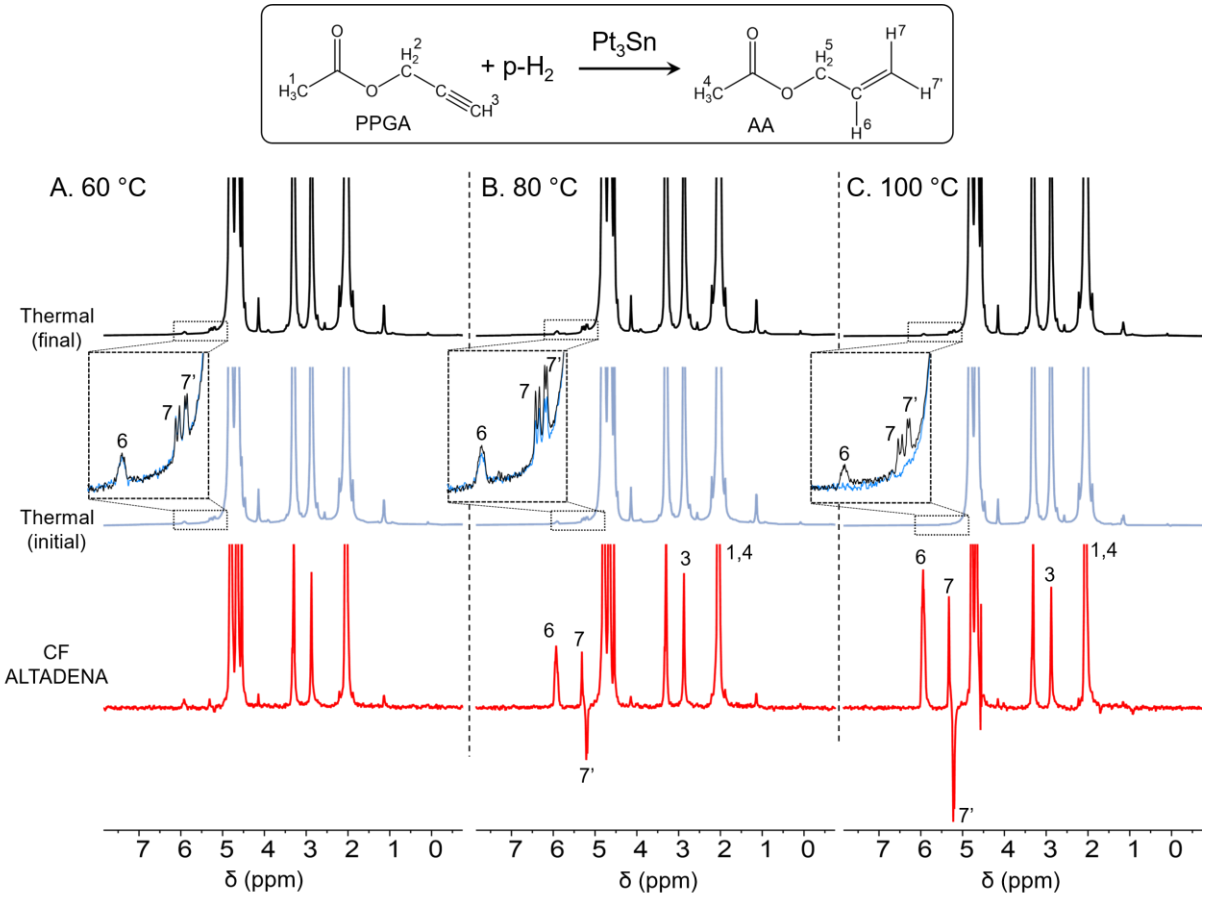

Figure 8. ^{1}H NMR spectra for the CF hydrogenation of PPGA with 99% p-H_2 catalyzed by Pt_3Sn@$mSiO_2$ at A) 60 °C, B) 80 °C, and C) 100 °C. The liquid flow rate was 2.0 mL/min. Bottom traces: the representative CF ALTADENA spectra taken from the steady-state region in the array experiment acquired in a single transient. Middle traces: thermally polarized spectra acquired before starting the array experiment, 32 transients, recycle delay d1=60 s. Top traces: thermally polarized spectra acquired after completion of the array experiment, 32 transients, recycle delay d1=60 s. All spectra are displayed with the same vertical scale. In the zoomed regions of the thermally polarized spectra, the relative change in the AA concentrations due to hydrogenation at each temperature is evident by comparing the initial spectrum (in blue) with the final spectrum (in black) acquired after completion of the array. Note that because the experiments were performed in the order 100, 80, and 60 °C, and so the initial concentration of AA increases in the same order.

Table 3. The per-pass conversion of PPGA to AA, AA signal enhancement, and polarization yield obtained at constant flow rate of 2.0 mL/min using the Pt_3Sn@$mSiO_2$ catalyst.

Temperature (°C)	χ_{AA}^{pp} (%)	ε_{AA}	$\chi_{AA}^{pp} \cdot \varepsilon_{AA}$
60	0	N/A	0
80	0.03 ± 0.004	626 ± 26	0.19 ± 0.01
100	0.16 ± 0.010	212 ± 3	0.34 ± 0.01

3.3 Variable Flow Rate Study

After optimizing the temperature, the flow rate dependence was performed at 1.0, 2.0, and 3.5 mL/min at 100 °C. The results are summarized in **Figure 9** and **Table 4**. The conversion follows the trend of 1.0 > 2.0 > 3.5 mL/min, while the signal enhancement follows the opposite trend. However, conversion and signal enhancement changed nonlinearly with the variation of liquid flow rate. The conversion decreased slower than the increase of the signal enhancement with flow rate, which is likely due to the combined effects of the shorter residence time and reduced spin-lattice relaxation during transport. Losses due to spin-lattice relaxation during transport from the reactor to the detection coil are reduced at higher flow rate, leading to increased signal enhancement. As a result, the maximum ALTADENA signal (polarization yield) is obtained at 2.0 mL/min.

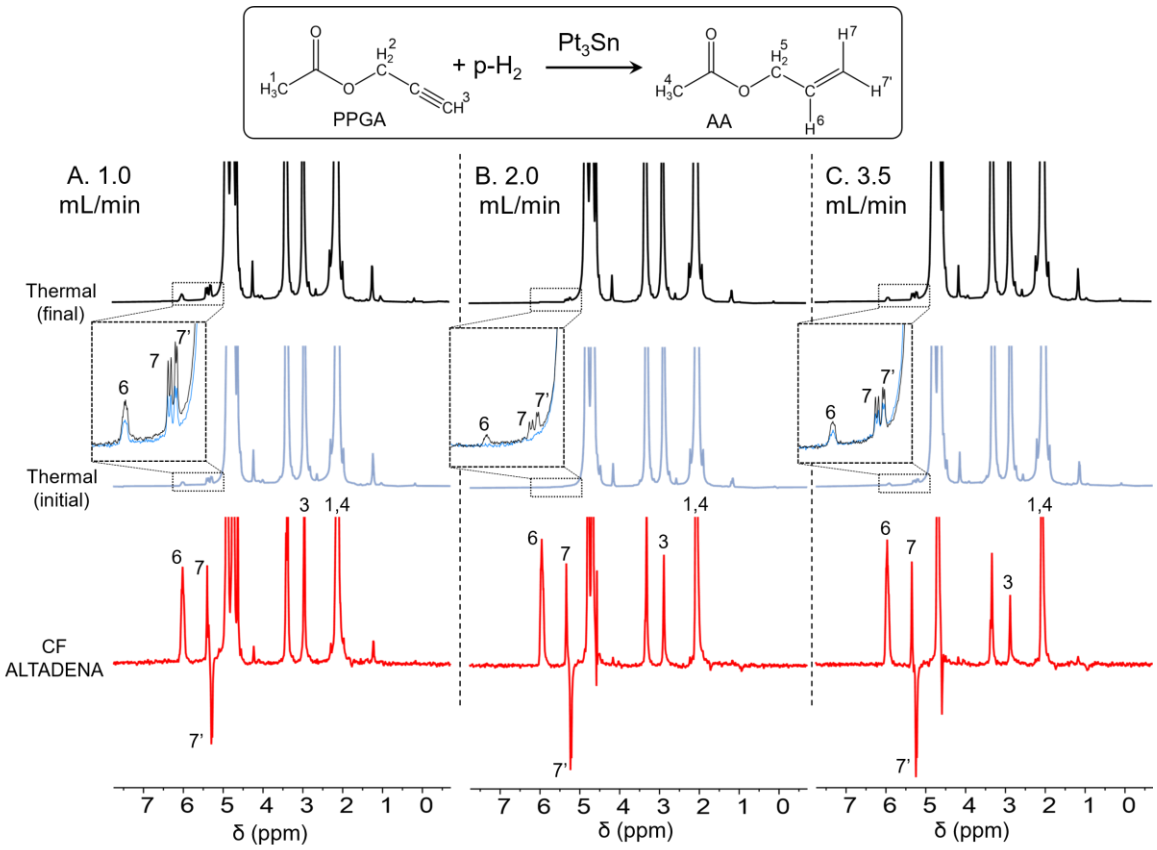

Figure 9. ^{1}H NMR spectra for the CF hydrogenation of PPGA with 99% p-H_2 catalyzed by Pt_3Sn@$mSiO_2$ at 100 °C, with liquid flow rates of A) 1.0 mL/min, B) 2.0 mL/min, and C) 3.5 mL/min. Bottom traces: the representative CF ALTADENA spectra acquired with a single transient during the steady-state condition in the array experiment. Middle traces: thermally polarized spectra acquired before the array experiment acquired with 32 transients and a recycle delay of d1=60 s. Top traces: thermally polarized spectra acquired after completion of the arrayed experiment (32 transients accumulated and d1=60 s). All spectra are displayed with the same vertical scale. In the zoomed regions of the thermally polarized spectra, the relative change in the AA concentrations due to hydrogenation at each flow rate is evident by comparing the initial spectrum (in blue) with the final spectrum (in black) acquired after completion of the array. Note that because the experiments were performed in the order 2.0, 3.5, and 1.0 mL/min, and so the initial concentration of AA increases in the same order.

Table 4. The results in the flow rate optimization experiments with a constant temperature at 100 °C.

Flow rate (mL/min)	χ_{AA}^{pp} (%)	ε_{AA}	$\chi_{AA}^{pp} \cdot \varepsilon_{AA}$
1.0	0.48 ± 0.03	59 ± 1	0.28 ± 0.006
2.0	0.16 ± 0.01	212 ± 3	0.34 ± 0.005
3.5	0.11 ± 0.01	282 ± 2	0.31 ± 0.01

3.4 Thermal Activation Study

The enduring continuous production of a stable hyperpolarized liquid stream by the CL-CF setup enables various types of systematic studies. We now demonstrate the temperature dependence of the activation of PPGA hydrogenation over $Pt_3Sn@mSiO_2$ and Rh/TiO_2-ANP catalysts. ALTADENA spectra were acquired in 5 °C steps from 100 °C to 50 °C ($Pt_3Sn@mSiO_2$) or 30 °C (Rh/TiO_2-ANP) while the substrate solution was recirculated at a constant rate of 2.0 mL/min. The integrals of the H^6 and H^{11} peaks are plotted against temperature in **Figure 10**. With increasing temperature, the ALTADENA signals of both H^6 and H^{11} increase exponentially, indicating the increase in reaction rate. Although the activation energy cannot be obtained by fitting the curve in the Arrhenius equation due to the change of signal enhancement, the minimum temperature to observe an ALTADENA signal is 65 °C and 35 °C with $Pt_3Sn@mSiO_2$ and Rh/TiO_2-ANP, respectively, indicating the lower activation energy of PPGA hydrogenation for the Rh/TiO_2-ANP catalyst.

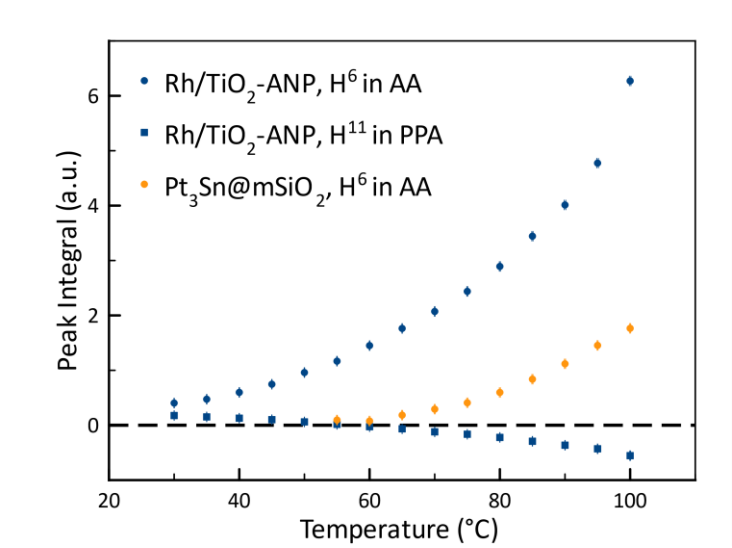

Figure 10. The temperature dependence of the ALTADENA signal of H^6 and H^{11} in the CF hydrogenation of PPGA catalyzed by Rh/TiO_2-ANP (blue) and $Pt_3Sn@mSiO_2$ iNPs (orange). The flow rate was 2.0 mL/min.

4. Conclusions

We demonstrated a novel closed loop continuous flow packed bed reactor system that achieved stable and enduring proton hyperpolarization of contaminant-free liquid allyl acetate using supported Rh and intermetallic Pt_3Sn nanoparticle catalysts. The system facilitates the efficient and cost-effective use of the hydrogenation substrate and deuterated solvent for optimization and systematic studies. The CL-CF catalytic reactor system features a liquid recirculation path, an HPLC pump, an all-metal packed bed reactor assembly, and an AF-2400 tube-in-tube vacuum degasser. A constant hyperpolarized stream was produced by CF hydrogenation of PPGA over the course of 22.5 minutes with observed signal

enhancements of up to 626 using $Pt_3Sn@mSiO_2$ catalysts and 99% p-H_2. The only factor that limited the longevity was the evaporation of solvent which is vented during bubbling. This could be easily mitigated by using an AF-2400 tube-in-tube gas dissolution device as in Ref. [14,19] instead of bubbling for dissolution of p-H_2. The Rh/TiO_2-ANP catalyst, which exhibited a significantly higher per-pass conversion, exhibited a 13.3% decay of the ALTADENA signal after 22.5 minutes of CF hydrogenation, with a signal enhancement of 80. We demonstrated the feasibility of performing systematic studies on heterogeneous hydrogenation with p-H_2 using the CL-CF setup. The temperature-dependent study of the ALTADENA NMR signal revealed threshold activation temperatures of 65 and 35 °C for the CF hydrogenation catalyzed by $Pt_3Sn@mSiO_2$ and Rh/TiO_2-ANP catalysts, respectively. Further work is needed to increase the per-pass conversion. This may entail increasing the pressure to increase the solubility of p-H_2, using higher temperatures to increase the reaction rate, using per-deuterated substrates to increase the spin-lattice relaxation time to allow for lower flow rates, and increasing the mass of catalyst. Additional challenges that must be overcome for in-vivo administration include the use of aqueous solvent, continuous flow polarization transfer to the carbonyl ^{13}C of the metabolite, and continuous flow chemical cleavage of the ester linkage, topics that will be addressed in future work.

5. Acknowledgements

This work was supported by NSF grants CHE-2108306/2108307 (CRB and WH), CBET- 1933723 (HHW and CRB) and the National High Magnetic Field Laboratory's User Collaborative Grant Program, which is supported by the National Science Foundation Cooperative Agreement No. DMR-1644779 and the State of Florida.

6. References

[1] A.B. Schmidt, C.R. Bowers, K. Buckenmaier, E.Y. Chekmenev, H. de Maissin, J. Eills, F. Ellermann, S. Glöggler, J.W. Gordon, S. Knecht, I. v. Koptyug, J. Kuhn, A.N. Pravdivtsev, F. Reineri, T. Theis, K. Them, J.-B. Hövener, Instrumentation for Hydrogenative Parahydrogen-Based Hyperpolarization Techniques, Anal Chem. 94 (2022) 479–502. https://doi.org/10.1021/acs.analchem.1c04863.

[2] J.B. Hovener, A.N. Pravdivtsev, B. Kidd, C.R. Bowers, S. Gloggler, K. v. Kovtunov, M. Plaumann, R. Katz-Brull, K. Buckenmaier, A. Jerschow, F. Reineri, T. Theis, R. v. Shchepin, S. Wagner, P. Bhattacharya, N.M. Zacharias, E.Y. Chekmenev, Parahydrogen-Based Hyperpolarization for

Biomedicine, Angewandte Chemie International Edition. 57 (2018) 11140–11162. https://doi.org/10.1002/anie.201711842.

[3] C.R. Bowers, D.P. Weitekamp, Transformation of Symmetrization Order to Nuclear-Spin Magnetization by Chemical Reaction and Nuclear Magnetic Resonance, Phys Rev Lett. 57 (1986) 2645–2648. https://doi.org/10.1103/PhysRevLett.57.2645.

[4] C.R. Bowers, D.P. Weitekamp, Parahydrogen and Synthesis Allow Dramatically Enhanced Nuclear Alignment, J Am Chem Soc. 109 (1987) 5541–5542. https://doi.org/10.1021/ja00252a049.

[5] R.W. Adams, J.A. Aguilar, K.D. Atkinson, M.J. Cowley, P.I.P. Elliott, S.B. Duckett, G.G.R. Green, I.G. Khazal, J. Lopez-Serrano, D.C. Williamson, Reversible interactions with para-hydrogen enhance NMR sensitivity by polarization transfer, Science (1979). 323 (2009) 1708–1711. https://doi.org/10.1126/science.1168877.

[6] S. Korchak, S. Mamone, S. Glöggler, Over 50 % 1H and 13C Polarization for Generating Hyperpolarized Metabolites—A para-Hydrogen Approach, ChemistryOpen. 7 (2018) 672–676. https://doi.org/10.1002/open.201800086.

[7] E. Cavallari, C. Carrera, S. Aime, F. Reineri, Metabolic Studies of Tumor Cells Using [1- 13 C] Pyruvate Hyperpolarized by Means of PHIP-Side Arm Hydrogenation, ChemPhysChem. 20 (2019) 318–325. https://doi.org/10.1002/cphc.201800652.

[8] L. Kaltschnee, A.P. Jagtap, J. McCormick, S. Wagner, L. Bouchard, M. Utz, C. Griesinger, S. Glöggler, Hyperpolarization of Amino Acids in Water Utilizing Parahydrogen on a Rhodium Nanocatalyst, Chemistry – A European Journal. 25 (2019) 11031–11035. https://doi.org/10.1002/chem.201902878.

[9] S. Mamone, A.P. Jagtap, S. Korchak, Y. Ding, S. Sternkopf, S. Glöggler, A Field-Independent Method for the Rapid Generation of Hyperpolarized [1-13C]Pyruvate in Clean Water Solutions for Biomedical Applications, Angewandte Chemie International Edition. (2022). https://doi.org/10.1002/ANIE.202206298.

[10] L. Dagys, A.P. Jagtap, S. Korchak, S. Mamone, P. Saul, M.H. Levitt, S. Glöggler, Nuclear Hyperpolarization of (1- 13C)-Pyruvate in Aqueous Solution by Proton-Relayed Side-Arm Hydrogenation, Analyst. 146 (2021) 1772–1778. https://doi.org/10.1039/D0AN02389B.

[11] F. Reineri, T. Boi, S. Aime, ParaHydrogen Induced Polarization of 13C carboxylate resonance in acetate and pyruvate, Nat Commun. 6 (2015) 5858. https://doi.org/10.1038/ncomms6858.

[12] M. v. Liberti, J.W. Locasale, The Warburg Effect: How Does it Benefit Cancer Cells?, Trends Biochem Sci. 41 (2016) 211–218. https://doi.org/10.1016/j.tibs.2015.12.001.

[13] S. Kadlecek, H. Shaghaghi, S. Siddiqui, H. Profka, M. Pourfathi, R. Rizi, The Effect of Exogenous Substrate Concentrations on True and Apparent Metabolism of Hyperpolarized Pyruvate in the Isolated Perfused Lung, NMR Biomed. 27 (2014) 1557–1570. https://doi.org/10.1002/nbm.3219.

[14] W.G. Hale, T.Y. Zhao, D. Choi, M.J. Ferrer, B. Song, H. Zhao, H.E. Hagelin-Weaver, C.R. Bowers, Toward Continuous-Flow Hyperpolarisation of Metabolites via Heterogenous Catalysis, Side-Arm-Hydrogenation, and Membrane Dissolution of Parahydrogen, ChemPhysChem. 22 (2021) 822–827. https://doi.org/10.1002/cphc.202100119.

[15] L. Bordonali, N. Nordin, E. Fuhrer, N. Mackinnon, J.G. Korvink, Parahydrogen based NMR hyperpolarisation goes micro: an alveolus for small molecule chemosensing, Lab Chip. 19 (2019) 503–512. https://doi.org/10.1039/C8LC01259H.

[16] S. Lehmkuhl, M. Wiese, L. Schubert, M. Held, M. Küppers, M. Wessling, B. Blümich, Continuous Hyperpolarization with Parahydrogen in a Membrane Reactor, Journal of Magnetic Resonance. 291 (2018) 8–13. https://doi.org/10.1016/J.JMR.2018.03.012.

[17] P. Štěpánek, C. Sanchez-Perez, V.V. Telkki, V. v. Zhivonitko, A.M. Kantola, High-Throughput Continuous-Flow System for SABRE Hyperpolarization, Journal of Magnetic Resonance. 300 (2019) 8–17. https://doi.org/10.1016/J.JMR.2019.01.003.

[18] J. Eills, W. Hale, M. Sharma, M. Rossetto, M.H. Levitt, M. Utz, High-Resolution Nuclear Magnetic Resonance Spectroscopy with Picomole Sensitivity by Hyperpolarization on a Chip, J Am Chem Soc. 141 (2019) 9955–9963. https://doi.org/10.1021/jacs.9b03507.

[19] P.M. TomHon, S. Han, S. Lehmkuhl, S. Appelt, E.Y. Chekmenev, M. Abolhasani, T. Theis, A Versatile Compact Parahydrogen Membrane Reactor, ChemPhysChem. 22 (2021) 2526–2534. https://doi.org/10.1002/CPHC.202100667.

[20] L.-S. Bouchard, S.R. Burt, M.S. Anwar, K. v Kovtunov, I. v Koptyug, A. Pines, NMR imaging of catalytic hydrogenation in microreactors with the use of para-hydrogen, Science (1979). 319 (2008) 442–445. https://doi.org/10.1126/science.1151787.

[21] E.W. Zhao, R. Maligal-Ganesh, C. Xiao, T.W. Goh, Z. Qi, Y. Pei, H.E. Hagelin-Weaver, W. Huang, C.R. Bowers, Silica-Encapsulated Pt-Sn Intermetallic Nanoparticles: A Robust Catalytic Platform for

Parahydrogen-Induced Polarization of Gases and Liquids, Angewandte Chemie - International Edition. 56 (2017) 3925–3929. https://doi.org/10.1002/anie.201701314.

[22] K. v Kovtunov, O.G. Salnikov, V. v Zhivonitko, I. v Skovpin, V.I. Bukhtiyarov, I. v Koptyug, Catalysis and Nuclear Magnetic Resonance Signal Enhancement with Parahydrogen, Top Catal. 59 (2016) 1686–1699. https://doi.org/10.1007/s11244-016-0688-6.

[23] V. v Zhivonitko, K. v Kovtunov, I.E. Beck, A.B. Ayupov, V.I. Bukhtiyarov, I. v Koptyug, Role of Different Active Sites in Heterogeneous Alkene Hydrogenation on Platinum Catalysts Revealed by Means of Parahydrogen-Induced Polarization, Journal of Physical Chemistry C. 115 (2011) 13386–13391. https://doi.org/10.1021/jp203398j.

[24] Y. Du, R. Behera, M. Maligal-Ganesh, Raghu V. Chen, T. Yunpu Zhao, W. Huang, C.R. Bowers, PtSn@mSiO2 Intermetallic Nanoparticles Catalyze Hydrogenation with an Unprecedented 20% Pairwise Selectivity for Parahydrogen Enhanced NMR, Journal of Physical Chemistry Letters. submitted (2022).

[25] E.W. Zhao, R. Maligal-Ganesh, Y. Du, T.Y. Zhao, J. Collins, T. Ma, L. Zhou, T.-W. Goh, W. Huang, C.R. Bowers, Surface-Mediated Hyperpolarization of Liquid Water from Parahydrogen, Chem. 4 (2018) 1387–1403. https://doi.org/10.1016/j.chempr.2018.03.004.

[26] M.G. Pravica, D.P. Weitekamp, Net NMR Alignment by Adiabatic Transport of Parahydrogen Addition Products to High Magnetic Field, Chem Phys Lett. 145 (1988) 255–258. https://doi.org/10.1016/0009-2614(88)80002-2.

[27] E.W. Zhao, H. Zheng, K. Ludden, Y. Xin, H.E. Hagelin-Weaver, C.R. Bowers, Strong Metal-Support Interactions Enhance the Pairwise Selectivity of Parahydrogen Addition over Ir/TiO_2, ACS Catal. 6 (2016). https://doi.org/10.1021/acscatal.5b02632.

[28] B. Song, D. Choi, Y. Xin, C.R. Bowers, H. Hagelin-Weaver, Ultra-Low Loading Pt/CeO 2 Catalysts: Ceria Facet Effect Affords Improved Pairwise Selectivity for Parahydrogen Enhanced NMR Spectroscopy , Angewandte Chemie. 133 (2021) 4084–4088. https://doi.org/10.1002/ange.202012469.

[29] R. v. Maligal-Ganesh, C. Xiao, T.W. Goh, L.L. Wang, J. Gustafson, Y. Pei, Z. Qi, D.D. Johnson, S. Zhang, F. Tao, W. Huang, A Ship-in-a-Bottle Strategy to Synthesize Encapsulated Intermetallic Nanoparticle Catalysts: Exemplified for Furfural Hydrogenation, ACS Catal. 6 (2016) 1754–1763. https://doi.org/10.1021/acscatal.5b02281.

[30] S. Gates-Rector, T. Blanton, The Powder Diffraction File: A Quality Materials Characterization Database, Powder Diffr. 34 (2019) 352–360. https://doi.org/10.1017/S0885715619000812.

[31] E.W. Zhao, R. Maligal-Ganesh, C. Xiao, T.-W. Goh, Z. Qi, Y. Pei, H.E. Hagelin-Weaver, W. Huang, C.R. Bowers, Silica-Encapsulated Pt-Sn Intermetallic Nanoparticles: A Robust Catalytic Platform for Parahydrogen-Induced Polarization of Gases and Liquids, Angewandte Chemie. 129 (2017) 3983–3987. https://doi.org/10.1002/ange.201701314.

[32] J. Fearon, G.W. Watson, Hydrogen Adsorption and Diffusion on Pt {111} and PtSn {111}, J Mater Chem. 16 (2006) 1989. https://doi.org/10.1039/b600250c.

[33] Y. Pei, M. Chen, X. Zhong, T.Y. Zhao, M.J. Ferrer, R. v. Maligal-Ganesh, T. Ma, B. Zhang, Z. Qi, L. Zhou, C.R. Bowers, C. Liu, W. Huang, Pairwise Semi-Hydrogenation of Alkyne to Cis-Alkene on Platinum-Tin Intermetallic Compounds, Nanoscale. 12 (2020) 8519–8524. https://doi.org/10.1039/d0nr00920b.